Available online at www.sciencedirect.com
SCIENCE DIRECT®
Journal of Solid State Chemistry 177 (2004) 1146–1156
JOURNAL OF SOLID STATE CHEMISTRY
http://elsevier.com/locate/jssc

Thermodynamic properties of ternary oxides in the system Ba–Fe–O using solid-state electrochemical cells with oxide and fluoride ion conducting electrolytes

S.K. Rakshit,* S.C. Parida, Ziley Singh, R. Prasad, and V. Venugopal

Fuel Chemistry Division, Bhabha Atomic Research Centre, RLG, Trombay, Mumbai 400 085, India

Received 21 July 2003; received in revised form 15 October 2003; accepted 26 October 2003

Abstract

The standard molar Gibbs energy of formations of $BaFe_{12}O_{19}$(s), $BaFe_2O_4$(s), $Ba_2Fe_2O_5$(s), $Ba_3Fe_2O_6$(s) and $Ba_5Fe_2O_8$(s) have been determined using solid-state electrochemical technique employing CaF_2(s) as an electrolyte. The reversible e.m.f. values have been measured in the temperature range from 970 to 1151 K. The oxygen chemical potential corresponding to three phase equilibria involving technologically important compound $BaFe_{12}O_{19}$(s) has been determined using solid-state electrochemical technique employing CSZ as an electrolyte from 1048 to 1221 K. The values of $\Delta_f G^0_m(T)$ for the above ternary oxides are given by

$$\Delta_f G^0_m(BaFe_{12}O_{19},\ s)/\text{kJ mol}^{-1}(\pm 0.6) = -5431.3 + 1.5317\,(T/\text{K}) \quad (970 \leqslant T/\text{K} \leqslant 1151)$$

$$\Delta_f G^0_m(BaFe_2O_4,\ s)/\text{kJ mol}^{-1}(\pm 1.3) = -1461.4 + 0.3745\,(T/\text{K}) \quad (970 \leqslant T/\text{K} \leqslant 1151)$$

$$\Delta_f G^0_m(Ba_2Fe_2O_5,\ s)/\text{kJ mol}^{-1}(\pm 1.4) = -2038.3 + 0.4433\,(T/\text{K}) \quad (970 \leqslant T/\text{K} \leqslant 1149)$$

$$\Delta_f G^0_m(Ba_3Fe_2O_6,\ s)/\text{kJ mol}^{-1}(\pm 1.5) = -2700.1 + 0.6090\,(T/\text{K}) \quad (969 \leqslant T/\text{K} \leqslant 1150)$$

and

$$\Delta_f G^0_m(Ba_5Fe_2O_8,\ s)/\text{kJ mol}^{-1}(\pm 1.6) = -3984.1 + 0.9300\,(T/\text{K}) \quad (973 \leqslant T/\text{K} \leqslant 1150)$$

The uncertainty estimates for $\Delta_f G^0_m$ includes the standard deviation in the e.m.f. and uncertainty in the data taken from the literature. An isothermal oxygen potential diagram for the system Ba–Fe–O was constructed at 1100 K based on the thermodynamic data obtained in this study.

Keywords: System Ba–Fe–O; Barium ferrites; Solid-state electrochemical cell; Fluoride ion conducting electrolyte; Oxide ion conducting electrolyte; Thermodynamic properties

1. Introduction

Ferrites with the hexagonal crystal structure are ferrimagnets that have technological importance for many applications such as read/write heads for high-speed digital recording, transformer cores, antennas and microwave circuits. A member of barium ferrites family ($BaFe_{12}O_{19}$) has long been used for magnetic recording as permanent magnets. The magnetic properties of barium ferrite ($BaFe_{12}O_{19}$) were first described by Went et al. [1] in 1952. The wide application of this material is mainly due to its low cost, high saturation magnetization, high Curie temperature and high coercivity associated with excellent stability and resistant to corrosion [2–4]. Smit and Wijn [5] denoted $BaFe_{12}O_{19}$ as BaM. It has the magnetoplumbite structure [6] where the hexagonal unit cell consists of 10 oxygen layers. The oxygen ions form a hexagonal or cubic closed packed lattice along the [001] direction. Numerous studies have been done on the phase relations in Ba–Fe–O ternary

*Corresponding author. Fax: 91-22-25505151.
E-mail addresses: swarup_kr@rediffmail.com (S.K. Rakshit), sureshp@apsara.barc.ernet.in (S.C. Parida).

0022-4596/$ - see front matter © 2003 Elsevier Inc. All rights reserved.
doi:10.1016/j.jssc.2003.10.021

system [7–16]. Goto and Takada [7] have reported three stable phases in this system, namely, $Ba_2Fe_2O_5$ ($2BaO \cdot Fe_2O_3 = B_2F$), $BaFe_2O_4$($BaO \cdot Fe_2O_3 = BF$) and the hexagonal $BaFe_{12}O_{19}$($BaO \cdot 6Fe_2O_3 = BaM$) in air at temperatures higher than 1273 K. Many other ternary compounds were also reported in this system including $BaFeO_{3-x}$ [9], $Ba_2FeO_{3.5}$ [10], $Ba_2FeO_{3.66}$ [11], Ba_2FeO_4 [9], $Ba_3Fe_2O_6$ (B_3F) [14] and $Ba_5Fe_2O_8$ (B_5F) [14]. The studies on the ternary oxides in Ba–Fe–O system are relevant in understanding the chemical interaction between fission product barium with iron of stainless steel in case of accident conditions in fast reactor fuels. Fuel Chemistry Division of Bhabha Atomic Research Centre has been carrying out extensive thermodynamic investigation on ternary oxides relevant to nuclear science and technology both by experiment and computer modeling.

Values of free energy of formation of ternary compounds are important for a rational treatment of numerous problems, for example, the ionic and electronic disorder in ternary oxides, and solid-state reactions between binary oxides. So far very few studies have reported the thermodynamic parameters for the system Ba–Fe–O. Pouillard et al. [14] have measured the total pressure in a closed system in a U-shaped manometer where $BaCO_3$(s) and Fe_2O_3(s) reacted to form various ternary phases. Assuming the total pressure was entirely due to CO_2, they [14] have determined the free energies associated with the solid-state reactions. Deo et al. [15] have determined the free energies of similar reactions in oxygen ambient by galvanic cell measurements using a BaF_2 solid electrolyte (a fluoride ion conductor) without accounting the solid solubility of BaO in BaF_2 solid electrolyte. Li et al. [16] have studied the stability of $BaFe_{12}O_{19}$ and $BaFe_2O_4$ between 973 to 1273 K by oxygen coulometric titration technique using yttria stabilized zirconia (YSZ) electrolyte. This temperature zone is important for the deposition of $BaFe_{12}O_{19}$(s) magnetic thin films. Li et al. [16] have constructed a section of Ba–Fe–O ternary phase diagram around the $BaFe_{12}O_{19}$(s) composition for 973–1273 K by taking their experimental values and that of earlier studies [14,15]. This phase diagram shows that compounds $BaFe_{12}O_{19}$(s), $BaFe_2O_4$(s), $Ba_2Fe_2O_5$(s), $Ba_3Fe_2O_6$(s) and $Ba_5Fe_2O_8$(s) are line compounds in the pseudo-binary system Fe_2O_3(s)–BaO(s). Many synthesis techniques such as sputtering, organometallic chemical vapor deposition (MOCVD), laser ablation and liquid phase epitaxy (LPE) have been tested for the growth of high quality BaM thin films. Most of these synthesis processes use low oxygen partial pressures ($<10^{-8}$ atm) and moderately high temperature. Hence for reproducible synthesis of BaM thin films with the desired structure and magnetic properties, information on oxygen potential and standard Gibbs energies of formation of the compound is required.

The reported results determined by earlier studies [14–16] show large discrepancies. Hence, in the present study, attempts have been made to determine the oxygen potentials and standard Gibbs energies of formation of various ternary compounds in the system Ba–Fe–O by employing solid-state electrochemical cells using calcia stabilized zirconia (CSZ, a oxide ion conductor) and CaF_2 (a fluoride ion conductor) as electrolytes. All the calculations are done assuming the ternary phases to be stoichiometric.

2. Experimental

2.1. Materials preparation

Stoichiometric proportion of preheated $BaCO_3$(s) (E. Merck AG, Germany, mass fraction purity 0.999) and Fe_2O_3(s) (E. Merck AG, Germany, mass fraction purity 0.999) were taken for the preparation of $BaFe_{12}O_{19}$(s), $BaFe_2O_4$(s), $Ba_2Fe_2O_5$(s), $Ba_3Fe_2O_6$(s) and $Ba_5Fe_2O_8$(s) and weighed accurately by an analytical balance (accuracy: 0.00001 g) and mixed homogeneously using an agate mortar and pestle and made into pellets using a steel die at a pressure of 100 MPa. Pellets were sintered at 973 K for 24 h and again grounded and pelletized and heated at 1273 K for 100 h in dry air. Pellets of all the compounds were further reground and heated at 1473 K for 48 h in dry air with one intermediate grinding. The products were identified by X-ray diffraction (XRD) analysis using a STOE Powder Diffractometer with Cu$K\alpha$ radiation.

Phase mixtures of $\{BaFe_{12}O_{19}(s) + Fe_2O_3(s) + BaF_2(s)\}$, $\{BaFe_2O_4(s) + BaFe_{12}O_{19}(s) + BaF_2(s)\}$, $\{Ba_2Fe_2O_5(s) + BaFe_2O_4(s) + BaF_2(s)\}$, $\{Ba_3Fe_2O_6(s) + Ba_2Fe_2O_5(s) + BaF_2(s)\}$ and $\{Ba_5Fe_2O_8(s) + Ba_3Fe_2O_6(s) + BaF_2(s)\}$ were mixed homogeneously and pelletized using a steel die at a pressure of 100 MPa for the e.m.f. measurements by solid-state electrochemical cell involving CaF_2(s) as an electrolyte. Pellets of different phase mixtures were first sintered at 1073 K in purified oxygen gas for 24 h. Oxygen gas was purified and dried by passing it through towers of silica gel, anhydrous magnesium perchlorate and molecular sieves successively. Pellet of phase mixture of $\{BaFe_{12}O_{19}(s) + Fe_3O_4(s) + BaFe_2O_4(s)\}$ was also prepared and sintered in purified argon gas at 1073 K for 24 h for the e.m.f. measurements by solid-state electrochemical cell having CSZ as an electrolyte to determine the oxygen chemical potential over the three phase mixture. The sintered pellets after the e.m.f. measurements were reexamined by XRD analysis and the phase compositions found unchanged.

2.2. Solid-state electrochemical techniques

2.2.1. Solid-state electrochemical cell with CaF_2 electrolyte

A schematic diagram of a fluoride cell used in this experiment is shown in Fig. 1. Optical grade single crystal of solid CaF_2 pellet of 6 mm dia and 3 mm thick (supplied by Solon Technologies, Inc., USA) was used as an electrolyte. It is a single compartment cell with provisions for passing purified oxygen gas during the experiment and to measure the temperature of the cell near the electrode/electrolyte interface. The experimental setup and the cell assembly used in this study have been explained in details by Prasad et al. [17]. Presence of moisture inside the cell can change the electrolytic properties of CaF_2 by producing HF(g) at high temperatures. Reaction of the electrolyte and/or electrode material with moisture may cause the growth of an insulating oxide layer which may subsequently affect the electrolyte-electrode contact or may modify the electrochemical reactions at the electrolyte-electrode interface, leading to mixed potentials arising due to ionic and electronic conductions. Hence, high purity oxygen gas at 10^5 Pa was allowed to pass through successive traps of BTS catalysts, molecular sieves, silica gels and anhydrous magnesium perchlorate for removal of traces of H_2(g) and moisture. An appropriate selection of the reference electrode is needed to ensure a reasonable accuracy of the thermodynamic values to be determined and a sufficiently high rate at which electrochemical equilibrium is reached at the interface of the electrodes. The use of oxides and fluorides of alkaline earth metals such as $\{CaO(s)+CaF_2(s)\}$ as reference electrode is very convenient as it is least hygroscopic and thermodynamic properties are well established. Levitskii [18] has reported that the solubility of oxides of alkaline earth metals in CaF_2(s) is very small. This permits one to assume that dissolving the oxides of alkaline earth metals at the contacts with the electrolyte leaves the activity of CaF_2 in the phases near to unity at the two reaction interfaces of the electrolyte. Conversely, dissolving CaF_2 in alkaline earth oxides does not affect the activity of the alkaline earth oxides in the electrodes. The reference electrode, the electrolyte and the sample electrode stacked one over another were kept in the isothermal temperature zone of a Kanthal wire wound resistance furnace. The furnace temperature was controlled within ± 1 K by using a proportional temperature controller. The reversible e.m.f.'s of the following solid-state galvanic cells were measured as a function of temperature from 970 to 1151 K.

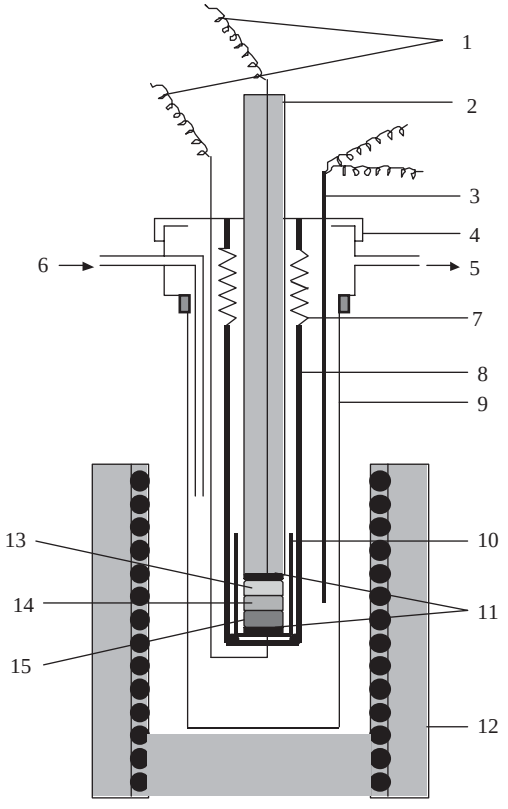

Fig. 1. Schematic diagram of the fluoride cell: (1) Pt wires; (2) alumina pressing tube; (3) thermocouple; (4) stainless-steel flange; (5) gas outlet; (6) gas inlet; (7) spring; (8) quartz holder; (9) quartz tube; (10) alumina cup; (11) Pt discs; (12) Kanthal wire wound furnace; (13) reference electrode; (14) CaF_2 electrolyte; and (15) sample electrode.

- Cell I: (−)Pt, $O_2(g)/\{CaO(s)+CaF_2(s)\}//CaF_2(s)//\{BaFe_{12}O_{19}(s)+BaF_2(s)+Fe_2O_3(s)\}/O_2(g)$, Pt (+)
- Cell II: (−)Pt, $O_2(g)/\{CaO(s)+CaF_2(s)\}//CaF_2(s)//\{BaFe_2O_4(s)+BaFe_{12}O_{19}(s)+BaF_2(s)\}/O_2(g)$, Pt (+)
- Cell III: (−)Pt, $O_2(g)/\{CaO(s)+CaF_2(s)\}//CaF_2(s)//\{Ba_2Fe_2O_5(s)+BaFe_2O_4(s)+BaF_2(s)\}/O_2(g)$, Pt (+)
- Cell IV: (−)Pt, $O_2(g)/\{Ba_3Fe_2O_6(s)+Ba_2Fe_2O_5(s)+BaF_2(s)\}//CaF_2(s)//\{CaO(s)+CaF_2(s)\}/O_2(g)$, Pt (+)
- Cell V: (−)Pt, $O_2(g)/\{Ba_5Fe_2O_8(s)+Ba_3Fe_2O_6(s)+BaF_2(s)\}//CaF_2(s)//\{CaO(s)+CaF_2(s)\}/O_2(g)$, Pt (+)

The cell temperature close to the electrodes was measured using a pre-calibrated chromel–alumel (ITS-90) thermocouple. The cell e.m.f. (± 0.02 mV) was measured by using a Keithley 614 electrometer (input impedance $10^{14}\,\Omega$). At low temperatures, stable values of e.m.f. were obtained nearly after 48 h whereas at successive higher temperatures stability in e.m.f. values were observed within 2–3 h.

2.2.2. Solid-state electrochemical cell with CSZ electrolyte

The experimental setup and the cell assembly for e.m.f. measurements used in this study have been discussed in details by Singh et al. [19]. A double compartment cell assembly was used where the inner compartment was separated from the outer one by use

of a CSZ electrolyte tube. CSZ tube with 15 mol% of CaO having 13 mm o.d., 9 mm i.d. and 380 mm long with a flat closed end was obtained from Nikatto Corporation, Japan. An inert environment was maintained through out the experiment by streams of purified argon gas passing through both the cell compartments. The argon gas was purified by passing it through towers containing the reduced form of BASF catalyst, molecular sieves, anhydrous magnesium perchlorate and hot uranium metal at 550 K. The reversible e.m.f.'s of the following solid-state galvanic cell has been measured as a function of temperature.

$$\text{Cell (VI)}: \ (-)\text{Pt}/\{\text{Ni(s)} + \text{NiO(s)}\}//\text{CSZ}//\{\text{BaFe}_{12}\text{O}_{19}\text{(s)} + \text{BaFe}_2\text{O}_4\text{(s)} + \text{Fe}_3\text{O}_4\text{(s)}\}/\text{Pt}(+).$$

The cell temperature (± 1 K) was maintained using a proportional temperature controller and the actual cell temperature near the electrode/electrolyte interface was measured by a pre-calibrated chromel/alumel thermocouple (ITS-90), and the cell e.m.f. (± 0.02 mV) was measured using a Keithley 614 electrometer (input impedance $10^{14}\,\Omega$). E.m.f. measurements were carried out in the temperature range 1050–1220 K. The reversibility of the solid-state electrochemical cell was ensured by micro-coulometric titration in both directions. A small quantity of current is passed ($\sim 100\,\mu$A for 5 min) through the cell in either direction. It was observed that the cell e.m.f. returned to its original value after removal of the applied voltage. The e.m.f. of the cell were also found to be independent of flow rate of the inert gas passing over both the electrodes of the cell in the range from 2 to 6 ml min^{-1}.

3. Results and discussion

3.1. Solid-state electrochemical measurements in fluoride cell

3.1.1. Standardization of cell

Prior to the e.m.f. measurement, the fluoride cell assembly (Fig. 1) was standardized using phase mixtures of $\{\text{CaO(s)} + \text{CaF}_2\text{(s)}\}$ and $\{\text{MgO(s)} + \text{MgF}_2\text{(s)}\}$ as two electrodes and CaF_2(s) as an electrolyte.

$$\text{Cell (VII)}: \ (-)\text{Pt}, \ \text{O}_2\text{(g)}/\{\text{CaO(s)} + \text{CaF}_2\text{(s)}\}//\text{CaF}_2\text{(s)}//\{\text{MgO(s)} + \text{MgF}_2\text{(s)}\}/\text{O}_2\text{(g)}, \ \text{Pt}(+).$$

The half-cell reactions at electrodes can be written as

$$\text{MgF}_2\text{(s)} + 2\,\text{e}^- + 1/2\text{O}_2\text{(g)} = \text{MgO(s)} + 2\text{F}^- \quad \text{(at the + ve electrode)} \qquad (1)$$

and

$$\text{CaO(s)} + 2\text{F}^- = \text{CaF}_2\text{(s)} + 2\,\text{e}^- + 1/2\text{O}_2\text{(g)} \quad \text{(at the } - \text{ ve electrode)}. \qquad (2)$$

The net cell reaction can be written as

$$\text{MgF}_2\text{(s)} + \text{CaO(s)} = \text{CaF}_2\text{(s)} + \text{MgO(s)}. \qquad (3)$$

The reversible e.m.f. values obtained due to the above reaction are listed in Table 1 and the variation of e.m.f. with temperature is shown in Fig. 2. It is evident from Fig. 2 that the temperature coefficient of e.m.f. for the above cell is very small. The e.m.f. data were least squares fitted to yield the following linear relation:

$$E/\text{V}\ (\pm 0.002) = 0.4121 - 3.7138 \times 10^{-5}(T/\text{K}). \qquad (4)$$

The Gibbs energy change of reaction (3) has been calculated from the general relation:

$$\Delta_r G^0 = -n \times F \times E \quad (\text{in J mol}^{-1}), \qquad (5)$$

where $n(=2)$ is the number of electrons involved in the half-cell reactions and F is the Faraday's constant ($F = 96486.4\,\text{C mol}^{-1}$) and E is the e.m.f. of the cell in

Table 1
Variation of e.m.f. as a function of temperature for cell: (–)Pt, O_2(g)/$\{\text{CaO(s)} + \text{CaF}_2\text{(s)}\}//\text{CaF}_2\text{(s)}//\{\text{MgO(s)} + \text{MgF}_2\text{(s)}\}/\text{O}_2$(g), Pt(+)

T/K	E/V	T/K	E/V
900	0.3813	1041	0.3730
921	0.3762	1060	0.3733
942	0.3780	1081	0.3690
960	0.3754	1101	0.3724
982	0.3749	1120	0.3680
1000	0.3755	1134	0.3717
1019	0.3741	1150	0.3714

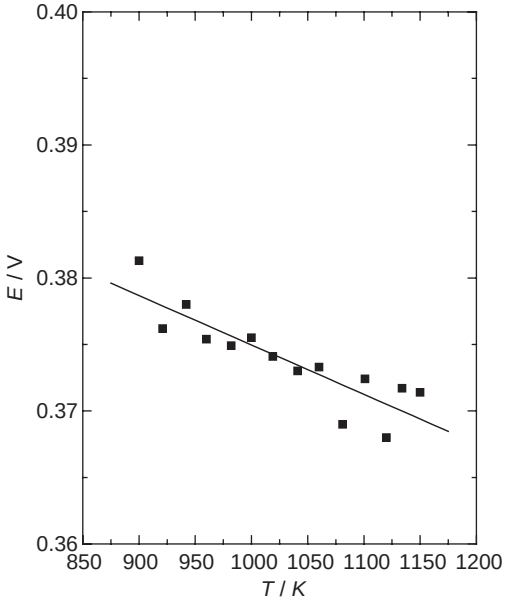

Fig. 2. Variation of e.m.f. as a function of temperature for the cell: (–)Pt, O_2(g)/$\{\text{CaO(s)} + \text{CaF}_2\text{(s)}\}//\text{CaF}_2\text{(s)}//\{\text{MgO(s)} + \text{MgF}_2\text{(s)}\}/\text{O}_2$(g), Pt(+).

volts (V). The values of $\Delta_r G^0(T)$ can be given as

$$\Delta_r G^0(T)/\text{kJ mol}^{-1}(\pm 1) = -79.5 + 7.1666 \times 10^{-3}(T/\text{K}). \quad (6)$$

The values of $\Delta_r G^0(T)$ for reaction (3) obtained in this study (Eq. 6) are in good agreement (within ± 2 kJ mol^{-1}) with those calculated using the values of $\Delta_f G^0_m(T)$ for CaF_2(s), MgF_2(s), MgO(s) and CaO(s) from Table 2.

3.1.2. $\Delta_f G^0_m(T)$ for $BaFe_{12}O_{19}$(s)

The reversible e.m.f. of cell (I) as a function of temperature are listed in Table 3 and the variation of e.m.f. with temperature is shown in Fig. 3. The half-cell reactions for cell (I) for the electrodes can be written as

$$6Fe_2O_3(s) + BaF_2(s) + 2e^- + 1/2O_2(g) = BaFe_{12}O_{19}(s) + 2F^- \quad \text{(at the + ve electrode)}. \quad (7)$$

and

$$CaO(s) + 2F^- = CaF_2(s) + 1/2O_2(g) + 2e^- \quad \text{(at the − ve electrode)}. \quad (8)$$

Hence, the net cell reaction can be written as

$$CaO(s) + 6Fe_2O_3(s) + BaF_2(s) = BaFe_{12}O_{19}(s) + CaF_2(s). \quad (9)$$

The e.m.f. data were least squares fitted to yield the following linear relation:

$$E/\text{V}(\pm 0.0009) = -0.1490 + 3.2154 \times 10^{-4}(T/\text{K}) \quad (970 \leqslant T/\text{K} \leqslant 1151). \quad (10)$$

The Gibbs energy change, $\Delta_r G^0(T)$ for the equilibrium reaction (9) has been calculated by using Eqs. (5) and (10). The results can be given by

$$\Delta_r G^0(T)/\text{kJ mol}^{-1}(\pm 0.4) = 28.7 - 0.0620(T/\text{K}) \quad (970 \leqslant T/\text{K} \leqslant 1151). \quad (11)$$

Table 2
Standard molar Gibbs energy of formation of the binary oxides and fluorides taken from literature

Compound	$\Delta_f G^0_m$/kJ mol^{-1} (900–1300 K)	Reference number
BaO(s)	$-561.4 + 0.1033 \cdot (T/\text{K})$	[21]
BaF_2(s)	$-1191.3 + 0.1628 \cdot (T/\text{K})$	[21]
MgO(s)	$-608.4 + 0.1151 \cdot (T/\text{K})$	[20]
MgF_2(s)	$-1123.5 + 0.1729 \cdot (T/\text{K})$	[20]
CaF_2(s)	$-1218.9 + 0.1618 \cdot (T/\text{K})$	[21]
CaO(s)	$-637.4 + 0.1065 \cdot (T/\text{K})$	[21]
NiO(s)	$-234.6 + 0.0854 \cdot (T/\text{K})$	[20]
$Fe_{0.947}O$(s)	$-263.4 + 0.0647 \cdot (T/\text{K})$	[21]
Fe_2O_3(s)	$-808.4 + 0.2477 \cdot (T/\text{K})$	[21]
Fe_3O_4(s)	$-1091.0 + 0.2989 \cdot (T/\text{K})$	[21]

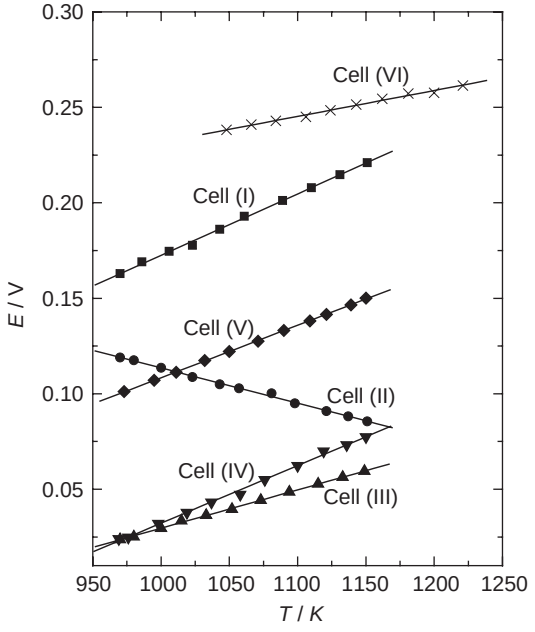

Fig. 3. Variation of e.m.f. as a function of temperature for cells (I)–(VI).

Table 3
Variation of e.m.f. as a function of temperature for cells (I)–(VI)

Cell (I)		Cell (II)		Cell (III)		Cell (IV)		Cell (V)		Cell (VI)	
T/K	E/V	T/K	E/V	T/K	E/V	T/K	E/V	T/K	E/V	T/K	E/V
970	0.1629	970	0.1190	970	0.0236	969	0.0240	973	0.1012	1048	0.2382
986	0.1691	980	0.1175	980	0.0251	976	0.0248	995	0.1071	1066	0.2410
1006	0.1746	1000	0.1136	1000	0.0295	998	0.0320	1011	0.1112	1084	0.2430
1023	0.1778	1023	0.1088	1015	0.0335	1019	0.0378	1032	0.1174	1106	0.2450
1043	0.1862	1043	0.1050	1033	0.0364	1037	0.0432	1050	0.1221	1124	0.2485
1061	0.1930	1057	0.1029	1052	0.0395	1058	0.0472	1071	0.1275	1143	0.2515
1089	0.2012	1081	0.1003	1073	0.0442	1076	0.0550	1090	0.1331	1162	0.2545
1110	0.2079	1098	0.0950	1094	0.0485	1100	0.0623	1109	0.1381	1181	0.2572
1131	0.2147	1121	0.0909	1115	0.0527	1119	0.0700	1121	0.1416	1200	0.2577
1151	0.2211	1137	0.0882	1133	0.0563	1136	0.0732	1139	0.1465	1221	0.2615
		1151	0.0856	1149	0.0595	1150	0.0774	1150	0.1501		

The standard molar Gibbs energy of formation from the elements, $\Delta_f G^0_m$ ($BaFe_{12}O_{19}$, s, T) has been obtained by using Eq. (11) and values of $\Delta_f G^0_m(T)$ for CaF_2(s), BaF_2(s), Fe_2O_3(s) and CaO(s) from Table 2 and is given by

$$\Delta_f G^0_m(BaFe_{12}O_{19},\ s)/kJ\,mol^{-1}(\pm 0.6) = -5431.3 + 1.5317 \times (T/K) \quad (970 \leqslant T/K \leqslant 1151). \tag{12}$$

The temperature independent and temperature dependent terms in Eq. (12) correspond to $\Delta_f H^0_m(T_{av})$ and $\Delta_f S^0_m(T_{av})$, respectively, with $T_{av} = 1060.5$ K.

3.1.3. $\Delta_f G^0_m(T)$ for $BaFe_2O_4$(s)

The reversible e.m.f. of cell (II) as a function of temperature are listed in Table 3 and the variation of e.m.f. with temperature is shown in Fig. 3. The half-cell reactions at the electrodes for cell (II) can be written as

$$BaFe_{12}O_{19}(s) + 5BaF_2(s) + 10\,e^- + 5/2O_2(g) = 6BaFe_2O_4(s) + 10\,F^- \quad (\text{at the } +\text{ve electrode}) \tag{13}$$

and

$$5CaO(s) + 10F^- = 5CaF_2(s) + 5/2O_2(g) + 10\,e^- \quad (\text{at the } -\text{ve electrode}). \tag{14}$$

Hence, the net cell reaction can be written as:

$$5CaO(s) + BaFe_{12}O_{19}(s) + 5BaF_2(s) = 6BaFe_2O_4(s) + 5CaF_2(s). \tag{15}$$

The e.m.f. data were least squares fitted to yield the following linear relation:

$$E/V\,(\pm 0.0006) = 0.2981 - 1.8456 \times 10^{-4}(T/K) \quad (970 \leqslant T/K \leqslant 1151). \tag{16}$$

The Gibbs energy change for the equilibrium reaction (15) has been calculated using Eqs. (5) and (16). The results can be given by

$$\Delta_r G^0(T)/kJ\,mol^{-1}(\pm 0.6) = -287.6 + 0.1781(T/K) \quad (970 \leqslant T/K \leqslant 1151). \tag{17}$$

The standard molar Gibbs energy of formation from the elements, $\Delta_f G^0_m$ ($BaFe_2O_4$, s, T) has been obtained by using Eq. (17) and values of $\Delta_f G^0_m(T)$ for CaF_2(s), BaF_2(s), and CaO(s) from Table 2 and $\Delta_f G^0_m$ ($BaFe_{12}O_{19}$, s, T) from Eq. (12) and is given by

$$\Delta_f G^0_m(BaFe_2O_4,\ s)/kJ\,mol^{-1}(\pm 1.3) = -1461.4 + 0.3745(T/K) \quad (970 \leqslant T/K \leqslant 1151) \tag{18}$$

The temperature independent and temperature dependent terms in Eq. (18) correspond to $\Delta_f H^0_m(T_{av})$ and $\Delta_f S^0_m(T_{av})$, respectively, with $T_{av} = 1060.5$ K.

3.1.4. $\Delta_f G^0_m(T)$ for $Ba_2Fe_2O_5$(s)

The reversible e.m.f. of cell (III) as a function of temperature are listed in Table 3 and the variation of e.m.f. with temperature is shown in Fig. 3. The half-cell reactions at the electrodes for cell (III) can be written as

$$BaFe_2O_4(s) + BaF_2(s) + 2\,e^- + 1/2O_2(g) = Ba_2Fe_2O_5(s) + 2F^- \quad (\text{at the } +\text{ve electrode}) \tag{19}$$

and

$$CaO(s) + 2F^- = CaF_2(s) + 1/2O_2(g) + 2e^- \quad (\text{at the } -\text{ve electrode}). \tag{20}$$

Hence, the net cell reaction can be written as

$$CaO(s) + BaFe_2O_4(s) + BaF_2(s) = Ba_2Fe_2O_5(s) + CaF_2(s). \tag{21}$$

The e.m.f. data were least squares fitted to yield the following linear relation:

$$E/V(\pm 0.0004) = -0.1712 + 2.0081 \times 10^{-4}(T/K) \quad (970 \leqslant T/K \leqslant 1149). \tag{22}$$

The Gibbs energy change for the equilibrium reaction (21) has been calculated using Eqs. (5) and (22). The results can be given by

$$\Delta_r G^0(T)/kJ\,mol^{-1}(\pm 0.2) = 33.0 - 0.0387\,(T/K) \quad (970 \leqslant T/K \leqslant 1149). \tag{23}$$

The standard molar Gibbs energy of formation from the elements, $\Delta_f G^0_m$ ($Ba_2Fe_2O_5$, s, T) has been obtained by using Eq. (23), values of $\Delta_f G^0_m(T)$ for CaF_2(s), BaF_2(s) and CaO(s) from Table 2 and $\Delta_f G^0_m$ ($BaFe_2O_4$, s, T) from Eq. (18) and is given by

$$\Delta_f G^0_m(Ba_2Fe_2O_5,\ s)/kJ\,mol^{-1}\,(\pm 1.4) = -2038.2 + 0.4433\,(T/K) \quad (970 \leqslant T/K \leqslant 1149). \tag{24}$$

The temperature independent and temperature dependent terms in Eq. (24) correspond to $\Delta_f H^0_m(T_{av})$ and $\Delta_f S^0_m(T_{av})$, respectively, with $T_{av} = 1059.5$ K.

3.1.5. $\Delta_f G^0_m(T)$ for $Ba_3Fe_2O_6$(s)

The reversible e.m.f. of cell (IV) as a function of temperature are listed in Table 3 and the variation of e.m.f. with temperature is shown in Fig. 3. The half-cell reactions at the electrodes for cell (IV) can be written as

$$CaF_2(s) + 1/2O_2(g) + 2\,e^- = CaO(s) + 2\,F^- \quad (\text{at the } +\text{ve electrode}) \tag{25}$$

and

$$Ba_3Fe_2O_6(s) + 2\,F^- = Ba_2Fe_2O_5(s) + BaF_2(s) + 2\,e^- + 1/2O_2(g) \quad (\text{at the } -\text{ve electrode}). \tag{26}$$

Hence, the net cell reaction can be written as

$$Ba_3Fe_2O_6(s) + CaF_2(s) = Ba_2Fe_2O_5(s) + BaF_2(s) + CaO(s). \quad (27)$$

The e.m.f. data were least squares fitted to yield the following linear relation:

$$E/V(\pm 0.001) = -0.2694 + 3.0165 \times 10^{-4}\,(T/K) \quad (969 \leqslant T/K \leqslant 1150). \quad (28)$$

The Gibbs energy change for the equilibrium reaction (27) has been calculated using Eqs. (5) and (28). The results can be given by

$$\Delta_r G^0(T)/kJ\,mol^{-1}(\pm 0.2) = 52.0 - 0.0582\,(T/K) \quad (969 \leqslant T/K \leqslant 1150). \quad (29)$$

The standard molar Gibbs energy of formation from the elements, $\Delta_f G^0_m$ ($Ba_3Fe_2O_6$, s, T) has been obtained by using Eq. (29), values of $\Delta_f G^0_m(T)$ for CaF_2(s), BaF_2(s) and CaO(s) from Table 2 and $\Delta_f G^0_m$ ($Ba_2Fe_2O_5$, s, T) from Eq. (24) and is given by

$$\Delta_f G^0_m(Ba_3Fe_2O_6,\ s)/kJ\,mol^{-1}(\pm 1.5) = -2700.1 + 0.6090\,(T/K) \quad (969 \leqslant T/K \leqslant 1150). \quad (30)$$

The temperature independent and temperature dependent terms in Eq. (30) correspond to $\Delta_f H^0_m(T_{av})$ and $\Delta_f S^0_m(T_{av})$, respectively, with $T_{av} = 1059.5$ K.

3.1.6. $\Delta_f G^0_m(T)$ for $Ba_5Fe_2O_8$(s)

The reversible e.m.f. of cell (V) as a function of temperature are listed in Table 3 and the variation of e.m.f. with temperature is shown in Fig. 3. The half-cell reactions at the electrodes for cell (V) can be written as:

$$2CaF_2(s) + O_2(g) + 4e^- = 2CaO(s) + 4F^- \quad (\text{at the } +\text{ve electrode}) \quad (31)$$

and

$$Ba_5Fe_2O_8(s) + 4F^- = Ba_3Fe_2O_6(s) + 2BaF_2(s) + 4e^- + O_2(g) \quad (\text{at the } -\text{ve electrode}). \quad (32)$$

Hence, the net cell reaction can be written as

$$Ba_5Fe_2O_8(s) + 2CaF_2(s) = Ba_3Fe_2O_6(s) + 2BaF_2(s) + 2CaO(s). \quad (33)$$

The e.m.f. data were least squares fitted to yield the following linear relation:

$$E/V(\pm 0.0002) = -0.1663 + 2.7472 \times 10^{-4}\,(T/K) \quad (973 \leqslant T/K \leqslant 1150). \quad (34)$$

The Gibbs energy change for the equilibrium reaction (33) has been calculated using Eqs. (5) and (34). The results can be given by

$$\Delta_r G^0(T)/kJ\,mol^{-1}(\pm 0.2) = 64.2 - 0.1060\,(T/K) \quad (973 \leqslant T/K \leqslant 1150). \quad (35)$$

The standard molar Gibbs energy of formation from the elements, $\Delta_f G^0_m$ ($Ba_5Fe_2O_8$, s, T) has been obtained by using Eq. (35), values of $\Delta_f G^0_m(T)$ for CaF_2(s), BaF_2(s), and CaO(s) from Table 2 and $\Delta_f G^0_m$ ($Ba_3Fe_2O_6$, s, T) from Eq. (30) and is given by

$$\Delta_f G^0_m(Ba_5Fe_2O_8,\ s)/kJ\,mol^{-1}(\pm 1.6) = -3984.1 + 0.9300\,(T/K)\ (973 \leqslant T/K \leqslant 1150). \quad (36)$$

The temperature independent and temperature dependent terms in Eq. (36) correspond to $\Delta_f H^0_m(T_{av})$ and $\Delta_f S^0_m(T_{av})$, respectively, with $T_{av} = 1061.5$ K.

3.2. Solid-state electrochemical measurements using oxide cell

The e.m.f. of the solid oxide galvanic cell is related to the partial pressure of oxygen at the two electrodes by the relation:

$$E = (RT/nF)\int_{p''(O_2)}^{p'(O_2)} t(O^{2-})\,d\ln p(O_2), \quad (37)$$

where E is the measured e.m.f. of the cell in volts, R ($=8.3144\,J\,K^{-1}\,mol^{-1}$) is the universal gas constant, n ($=4$) is the number of electrons participating in the electrode reaction, F ($=96486.4\,C\,mol^{-1}$) is the Faraday constant, T is the absolute temperature, $t(O^{2-})$ is the effective transference number of O^{2-} ion for the solid electrolyte combination, and $p'(O_2)$ and $p''(O_2)$ are the equilibrium oxygen partial pressures at the positive and negative electrodes, respectively. The transport number of oxygen ion in the solid electrolytes used in the present study is nearly unity ($t(O^{2-}) > 0.99$) at the oxygen pressures and temperatures covered. Hence, the e.m.f. of the cell is directly proportional to the logarithm of the ratio of partial pressures of oxygen at the electrodes:

$$E = (RT/4F)\ln\{p'(O_2)/p''(O_2)\}. \quad (38)$$

Thus,

$$4FE = RT\ln p'(O_2) - RT\ln p''(O_2). \quad (39)$$

where, $RT\ln p'(O_2)$ is the oxygen potential over the cathode and $RT\ln p''(O_2)$ is the oxygen chemical potential corresponding to the anode.

3.2.1. Oxygen chemical potential over the three-phase mixture {$BaFe_{12}O_{19}$(s)+$BaFe_2O_4$(s)+Fe_3O_4(s)} in cell (VI)

The reversible e.m.f. of the cell (VI) are listed in Table 3 and the variation of e.m.f. as a function of temperature

is shown in Fig. 3. The e.m.f. data were least squares fitted to yield the following linear relation:

$$E/\mathrm{V}\,(\pm 0.0007) = 0.0963 + 1.3544 \times 10^{-4}\,(T/\mathrm{K}) \quad (1048 \leqslant T/\mathrm{K} \leqslant 1221). \tag{40}$$

For the equilibrium reaction

$$6/5\mathrm{BaFe_2O_4(s)} + 4\mathrm{Fe_3O_4(s)} + \mathrm{O_2(g)} = 6/5\mathrm{BaFe_{12}O_{19}(s)}. \tag{41}$$

The oxygen chemical potential over the three-phase mixtures $\{\mathrm{BaFe_{12}O_{19}(s)} + \mathrm{BaFe_2O_4(s)} + \mathrm{Fe_3O_4(s)}\}$ has been calculated using Eq. (40) and the value of $\Delta\mu(\mathrm{O_2})$ for the phase mixture $\{\mathrm{Ni(s)} + \mathrm{NiO(s)}\}$ from Table 2 and can be represented as

$$\Delta\mu(\mathrm{O_2})/\mathrm{kJ\,mol^{-1}}\,(\pm 0.6) = -426.4 + 0.2187\,(T/\mathrm{K}) \quad (1048 \leqslant T/\mathrm{K} \leqslant 1221). \tag{42}$$

Li et al. [16] have measured the oxygen chemical potential over the three phase mixture $\{\mathrm{BaFe_{12}O_{19}(s)} + \mathrm{BaFe_2O_4(s)} + \mathrm{Fe_3O_4(s)}\}$ in the temperature range from 973 to 1273 K by oxygen coulometric titration technique using a solid-state electrochemical cell. The values of $\Delta\mu(\mathrm{O_2})$ obtained in this study are compared with those obtained by Li et al. [16] in Fig. 4. It is apparent that the results obtained by Li et al. [16] show large discrepancies from those reported in this study. The partial molar entropy of oxygen in equilibrium with the three condensed phases reported by Li et al. [16] is unacceptably low ($-576\,\mathrm{J\,K^{-1}\,mol^{-1}}$).

The values of $\Delta_f G^0_m(\mathrm{BaFe_{12}O_{19}}, \mathrm{s})$ have been obtained by using Eq. (42), values of $\Delta_f G^0_m(\mathrm{BaFe_2O_4}, \mathrm{s})$ from Eq. (18) and values of $\Delta_f G^0_m(\mathrm{Fe_3O_4}, \mathrm{s})$ from Table 2. The standard molar Gibbs energy of formation of $\mathrm{BaFe_{12}O_{19}(s)}$ from elements in the temperature range 1048–1221 K is given by

$$\Delta_f G^0_m(\mathrm{BaFe_{12}O_{19}},\ \mathrm{s})/\mathrm{kJ\,mol^{-1}}\,(\pm 0.6) = -5453.3 + 1.5530\,(T/\mathrm{K}). \tag{43}$$

The temperature independent and temperature dependent terms in Eq. (43) correspond to $\Delta_f H^0_m(T_{av})$ and $\Delta_f S^0_m(T_{av})$, respectively, with $T_{av} = 1135\,\mathrm{K}$.

3.3. Comparison of Gibbs energy of formation of $BaFe_{12}O_{19}(s)$, $BaFe_2O_4(s)$, $Ba_2Fe_2O_5(s)$, $Ba_3Fe_2O_6(s)$ and $Ba_5Fe_2O_8(s)$ from the elements and from the constituent oxides

The Gibbs energy of formations of $\mathrm{BaFe_{12}O_{19}(s)}$, $\mathrm{BaFe_2O_4(s)}$, $\mathrm{Ba_2Fe_2O_5(s)}$, $\mathrm{Ba_3Fe_2O_6(s)}$ and $\mathrm{Ba_5Fe_2O_8(s)}$ from the elements have been calculated. It has been observed that the Gibbs energy of formation of $\mathrm{BaFe_{12}O_{19}(s)}$ determined by the fluoride cell and the oxide cell were in close agreement with that from Deo et al. [15] where as that from Pouillard et al. [14] and Li et al. [16] were more negative by 30 and 100 $\mathrm{kJ\,mol^{-1}}$, respectively. Hence, it has been decided to carryout a least squares regression analysis of the data obtained by fluoride cell (Eq. (12)), oxide cell (Eq. (43)) and those from Deo et al. [15]. The combined fit yields the following linear relation:

$$\Delta_f G^0_m(\mathrm{BaFe_{12}O_{19}},\ \mathrm{s})/\mathrm{kJ\,mol^{-1}}\,(\pm 2.5) = -5475.0 + 1.5724\,(T/\mathrm{K}) \quad (970 \leqslant T/\mathrm{K} \leqslant 1221). \tag{44}$$

Similarly, the standard molar Gibbs energy of formation $\mathrm{BaFe_2O_4(s)}$ and $\mathrm{Ba_2Fe_2O_5(s)}$ from the elements have been calculated by least squares regression analysis of the data obtained in this study and those reported by Deo et al. [15]. The combined fit yields the following linear relations:

$$\Delta_f G^0_m(\mathrm{BaFe_2O_4},\ \mathrm{s})/\mathrm{kJ\,mol^{-1}}\,(\pm 0.8) = -1457.9 + 0.3705\,(T/\mathrm{K}) \quad (970 \leqslant T/\mathrm{K} \leqslant 1290) \tag{45}$$

$$\Delta_f G^0_m(\mathrm{Ba_2Fe_2O_5},\ \mathrm{s})/\mathrm{kJ\,mol^{-1}}\,(\pm 5.3) = -2061.6 + 0.4698\,(T/\mathrm{K}) \quad (970 \leqslant T/\mathrm{K} \leqslant 1300). \tag{46}$$

It has been observed that the values of $\Delta_f G^0_m(T)$ for $\mathrm{Ba_3Fe_2O_6(s)}$ and $\mathrm{Ba_5Fe_2O_8(s)}$ reported by Pouillard et al. [14] are not in agreement with this study. Hence, the values of $\Delta_f G^0_m(T)$ for these two oxides obtained in this

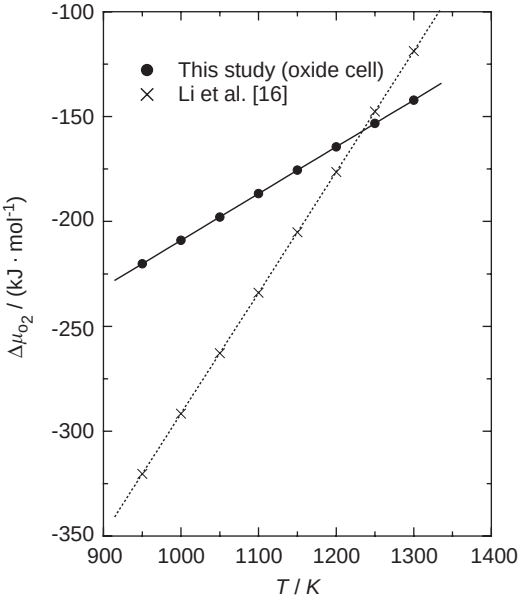

Fig. 4. Comparison of values of $\Delta\mu(\mathrm{O_2})$ for the reaction: $6/5\mathrm{BaFe_2O_4(s)} + 4\mathrm{Fe_3O_4(s)} + \mathrm{O_2(g)} = 6/5\mathrm{BaFe_{12}O_{19}(s)}$.

Table 4
Comparison of molar Gibbs energy of formation of ternary compounds of Ba–Fe–O system from its component oxides

Compounds	$\Delta_{ox}G^0/kJ\,mol^{-1} = A + B(T/K)$		Temperature range (K)	Reference
	A	*B*		
$BaFe_{12}O_{19}$(s)	−63.5	−0.0171	970–1221	This study
	−105.0	−0.0032	860–1014	[14]
	−124.2	0.0393	963–1123	[15]
	−456.3	−0.6312	973–1273	[16]
$BaFe_2O_4$(s)	−88.2	0.0195	970–1290	This study
	−90.5	0.0020	925–1096	[14]
	−84.7	0.0155	1025–1290	[15]
$Ba_2Fe_2O_5$(s)	−130.5	0.0155	970–1300	This study
	−155.0	0.0163	1230–1350	[14]
	−153.8	0.0420	1200–1300	[15]
$Ba_3Fe_2O_6$(s)	−207.8	0.0514	969–1150	This study
	−271.8	0.0887	1200–1350	[14]
$Ba_5Fe_2O_8$(s)	−369.1	0.1658	973–1150	This study
	−418.3	0.1585	1096–1368	[14]

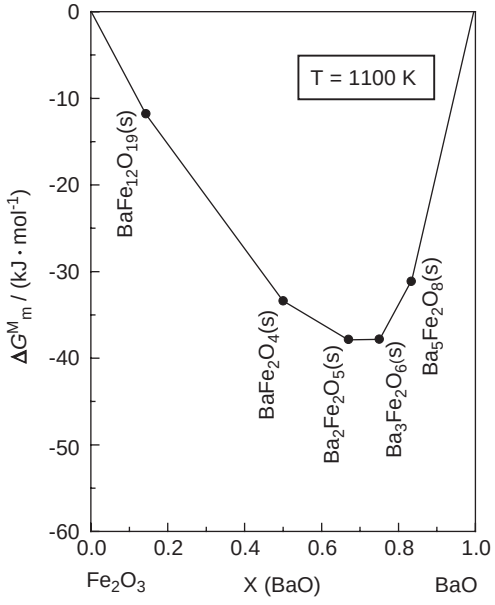

Fig. 5. Gibbs energy of mixing of ternary compounds in the system Ba–Fe–O as a function of temperature.

study by fluoride cell measurements (Eqs. (30) and (36)) have been selected for further calculation.

The molar Gibbs energy of formation from the component oxides, $\Delta_{ox}G^0_m(T)$, for the ternary compounds are calculated by using the values of $\Delta_f G^0_m(T)$ for BaO(s) and Fe_2O_3(s) from Table 2 and those for $BaFe_{12}O_{19}$(s), $BaFe_2O_4$(s), $Ba_2Fe_2O_5$(s), $Ba_3Fe_2O_6$(s) and $Ba_5Fe_2O_8$(s) from Eqs. (44–46), (30) and (36), respectively. The values of $\Delta_{ox}G^0_m(T)$ thus obtained are summarized in Table 4.

The Gibbs energy of mixing for the system BaO–Fe_2O_3 at 1100 K is shown in Fig. 5 as a function of composition of BaO(s). The values of Gibbs energy of mixing for each ternary oxide are obtained by dividing its standard molar Gibbs energy of formation from the component binary oxides by the number of molecules of the binary oxides present in the compound. It is evident from the figure that $BaFe_{12}O_{19}$(s) is marginally stable relative to its neighbors at 1100 K.

3.4. Construction of isothermal oxygen potential diagram

In ternary systems containing a volatile component such as oxygen, it is useful to visualize phase relations as a function of the chemical potential or partial pressure of the volatile species. The oxygen chemical potential of the gas phase can readily be controlled by adjusting the composition of the gas. In isothermal oxygen potential diagram the phase relations are represented as a function of partial pressure of oxygen. The composition variable is the cationic fraction $\eta_{Ba}/(\eta_{Ba} + \eta_{Fe})$, where η_i represents moles of component '*i*'. Since oxygen is not included in the composition parameter, information on oxygen nonstoichiometry cannot be displayed in this type of diagram. Nevertheless, the diagram provides useful information on the oxygen potential range for the stability of the various phases. The diagram is complementary to the conventional Gibbs triangle representation of phase relations in ternary systems, where the composition of each phase can be unambiguously displayed. All the topological rules of construction for conventional binary temperature-composition phase diagrams are applicable to the oxygen potential

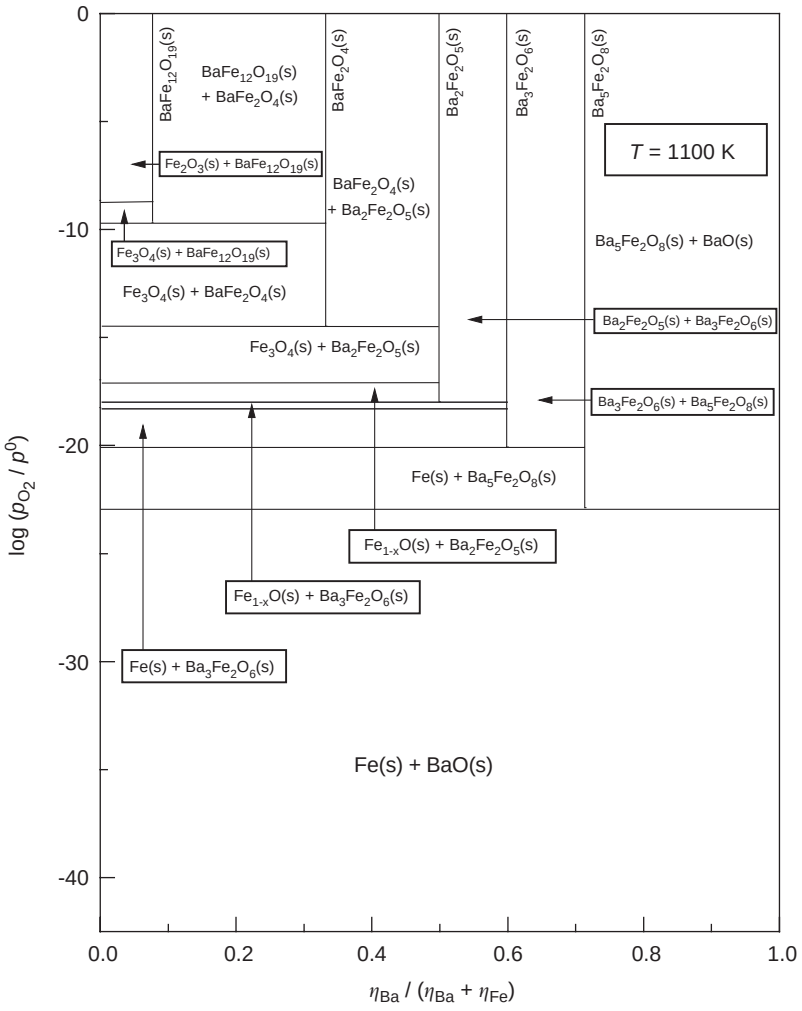

Fig. 6. Isothermal oxygen potential diagram for the system Ba–Fe–O at 1100 K.

diagrams. The oxygen potential diagram for the system Ba–Fe–O at 1100 K, computed from the results of this study and the data for the binary systems Ba–O and Fe–O from Table 2, is shown in Fig. 6. When three condensed phases coexist with a gas phase at equilibrium in the ternary system Ba–Fe–O, the system is univariant; at a fixed temperature, three condensed phases coexist only at a unique partial pressure of oxygen. Therefore, horizontal lines on the diagram represent three-phase equilibrium. It is evident from Fig. 6 that on reducing the oxygen partial pressure at 1100 K, $BaFe_{12}O_{19}$(s) dissociates first to Fe_3O_4(s) and $BaFe_2O_4$(s), followed by dissociation of $BaFe_2O_4$(s) to $Ba_2Fe_2O_5$(s) and Fe_3O_4(s), dissociation of $Ba_2Fe_2O_5$(s) to $Ba_3Fe_2O_6$(s) and $Fe_{1-x}O$(s), dissociation of $Ba_3Fe_2O_6$(s) to $Ba_5Fe_2O_8$(s) and Fe(s) and dissociation of $Ba_5Fe_2O_8$(s) to Fe(s) and BaO(s). According to ASM handbook [22], no intermetallics or alloy formation are reported in the system Ba–Fe. Hence alloy-oxide equilibria are not incorporated in the oxygen potential diagram. Similar oxygen potential diagrams at other temperatures can readily be computed from the thermodynamic data if required for a specific application.

4. Conclusion

Ternary oxides in the systems Ba–Fe–O have been prepared using usual solid-state route. The products have been characterized by using XRD analysis. The standard molar Gibbs energy of formations of ternary compounds have been calculated from the values of e.m.f. obtained from solid-state electrochemical cells employing oxide and fluoride electrolytes. The oxygen chemical potential over the three phase mixture {$BaFe_{12}O_{19}$(s) + $BaFe_2O_4$(s) + Fe_3O_4(s)} has been directly measured from the oxide cell. The standard molar Gibbs energy of formation of all the ternary oxides from their component binary oxides has been calculated. Gibbs energy of mixing for all the ternary compounds has been calculated. An isothermal oxygen potential diagram has been constructed for the system Ba–Fe–O at 1100 K.

Acknowledgments

The authors are thankful to Dr. K.D. Singh Mudher for assisting in X-ray diffraction analysis.

References

[1] J.J. Went, G.W. Rathenau, E.W. Gorter, G.W. Vanosterhout, Ferroxdure, a class of permanent magnetic materials, Philips Tech. Rev. 13 (7) (1951–52) 194.
[2] P. Campbell, Permanent magnetic materials and their application, Cambridge University Press, Cambridge, 1994.
[3] X. Liu, J. Nang, L.M. Gan, S.C. Ng, J. Ding, J. Magn. Magn. Mater. 184 (1998) 344.
[4] R.G. Simmons, IEEE Trans. Magn. 25 (1989) 4051.
[5] J. Smit, H.P.J. Wijn, Ferrites,, Wiley, New York, 1959.
[6] V. Adelskold, Arkiv Kemi Mineral. Geol. 12A (1938) 1.
[7] Y. Goto, T. Takada, J. Am. Ceram. Soc. 43 (1960) 150.
[8] H.J. Vanhook, J. Am. Ceram. Soc. 47 (1964) 579.
[9] T. Negas, R.S. Roth, J. Res. Natl. Bur. Stand. Sec. A 73 (1969) 426.
[10] M. Montorsi, P. Appenndino, Atti. Sci. Torino. Cl. Sci. Fis. Mat. Nat. 113 (1979) 479.
[11] B.T. Shirk, Mater. Res. Bull. V (1970) 771.
[12] G. Sloccari, J. Am. Ceram. Soc. 56 (1973) 489.
[13] J.C. Boivin, D. Thomas, G. Pouillard, P. Perrot, J. Solid State Chem. 29 (1979) 101.
[14] G. Pouillard, M. Shamsul Alam, M.-C. Trinel-Dufour, P. Perrot, J. Chem. Res. (m) (1981) 1720;
G. Pouillard, M. Shamsul Alam, M.-C. Trinel-Dufour, P. Perrot, J. Chem. Res. Synop. 5 (1981) 136.
[15] B. Deo, J.S. Kachhawaka, V.B. tare, Metall. Trans. B 7B (1976) 405.
[16] J. Li, T.M. Gur, R. Sinclair, S.S. RosenBlum, H. Hayashi, J. Mater. Res. 9 (6) (1994) 1499.
[17] R. Prasad, S. Dash, S.C. Parida, Z. Singh, V. Venugopal, J. Nucl. Mater. 312 (2003) 1.
[18] V.A. Levitskii, J. Solid State Chem. 25 (1978) 9.
[19] Z. Singh, S. Dash, R. Prasad, D.D. Sood, J. Alloys Compounds 215 (1994) 303.
[20] G.V. Belov, B.G. Trusov, ASTD table, Computer-aided Reference book, in: Thermodynamical, Thermochemical and Thermophysical properties of species, version2 (C) (1983–95), Moscow.
[21] I. Barin, Thermochemical Data of Pure Substances, Vol. I & II, (3rd Edition) VCH Publishers, New York, 1995.
[22] ASM Intern. Handbook, Binary Alloy Phase Diagrams, (2nd Edition) Plus updates, 1990.